

3-1-2022

NGC 5846-UDG1: A Galaxy Formed Mostly by Star Formation in Massive, Extremely Dense Clumps of Gas

Shany Danieli
Princeton University

Pieter Van Dokkum
Yale University

Sebastian Trujillo-Gomez
Astronomisches Rechen-Institut

J. M.Diederik Kruijssen
Astronomisches Rechen-Institut

Aaron J. Romanowsky
San Jose State University, aaron.romanowsky@sjsu.edu

See next page for additional authors

Follow this and additional works at: https://scholarworks.sjsu.edu/faculty_rsca

Recommended Citation

Shany Danieli, Pieter Van Dokkum, Sebastian Trujillo-Gomez, J. M.Diederik Kruijssen, Aaron J. Romanowsky, Scott Carlsten, Zili Shen, Jiaxuan Li, Roberto Abraham, Jean Brodie, Charlie Conroy, Jonah S. Gannon, and Johnny Greco. "NGC 5846-UDG1: A Galaxy Formed Mostly by Star Formation in Massive, Extremely Dense Clumps of Gas" *Astrophysical Journal Letters* (2022). <https://doi.org/10.3847/2041-8213/ac590a>

This Article is brought to you for free and open access by SJSU ScholarWorks. It has been accepted for inclusion in Faculty Research, Scholarly, and Creative Activity by an authorized administrator of SJSU ScholarWorks. For more information, please contact scholarworks@sjsu.edu.

Authors

Shany Danieli, Pieter Van Dokkum, Sebastian Trujillo-Gomez, J. M.Diederik Kruijssen, Aaron J. Romanowsky, Scott Carlsten, Zili Shen, Jiaxuan Li, Roberto Abraham, Jean Brodie, Charlie Conroy, Jonah S. Gannon, and Johnny Greco



NGC 5846-UDG1: A Galaxy Formed Mostly by Star Formation in Massive, Extremely Dense Clumps of Gas

Shany Danieli^{1,2,12} , Pieter van Dokkum³ , Sebastian Trujillo-Gomez⁴ , J. M. Diederik Kruijssen⁴ ,
Aaron J. Romanowsky^{5,6} , Scott Carlsten¹ , Zili Shen³ , Jiakuan Li¹ , Roberto Abraham^{7,8} , Jean Brodie^{6,9} ,
Charlie Conroy¹⁰ , Jonah S. Gannon⁹ , and Johnny Greco¹¹ 

¹ Department of Astrophysical Sciences, 4 Ivy Lane, Princeton University, Princeton, NJ 08544, USA; sdanieli@astro.princeton.edu, shanyil@gmail.com

² Institute for Advanced Study, 1 Einstein Drive, Princeton, NJ 08540, USA

³ Department of Astronomy, Yale University, New Haven, CT 06511, USA

⁴ Astronomisches Rechen-Institut, Zentrum für Astronomie der Universität Heidelberg, Monchhofstraße 12-14, D-69120 Heidelberg, Germany

⁵ Department of Physics and Astronomy, San José State University, San Jose, CA 95192, USA

⁶ University of California Observatories, 1156 High Street, Santa Cruz, CA 95064, USA

⁷ Department of Astronomy and Astrophysics, University of Toronto, Toronto, ON M5S 3H4, Canada

⁸ Dunlap Institute for Astronomy and Astrophysics, University of Toronto, Toronto, ON M5S 3H4, Canada

⁹ Centre for Astrophysics & Supercomputing, Swinburne University of Technology, Hawthorn, VIC 3122, Australia

¹⁰ Harvard-Smithsonian Center for Astrophysics, 60 Garden Street, Cambridge, MA, USA

¹¹ Center for Cosmology and AstroParticle Physics (CCAPP), The Ohio State University, Columbus, OH 43210, USA

Received 2021 November 29; revised 2022 February 18; accepted 2022 February 23; published 2022 March 14

Abstract

It has been shown that ultra-diffuse galaxies (UDGs) have higher specific frequencies of globular clusters, on average, than other dwarf galaxies with similar luminosities. The UDG NGC 5846-UDG1 is among the most extreme examples of globular cluster-rich galaxies found so far. Here we present new Hubble Space Telescope observations and analysis of this galaxy and its globular cluster system. We find that NGC 5846-UDG1 hosts 54 ± 9 globular clusters, three to four times more than any previously known galaxy with a similar luminosity and higher than reported in previous studies. With a galaxy luminosity of $L_{V,\text{gal}} \approx 6 \times 10^7 L_{\odot}$ ($M_{\star} \approx 1.2 \times 10^8 M_{\odot}$) and a total globular cluster luminosity of $L_{V,\text{GCs}} \approx 7.6 \times 10^6 L_{\odot}$, we find that the clusters currently comprise $\sim 13\%$ of the total light. Taking into account the effects of mass loss from clusters during their formation and throughout their lifetime, we infer that most of the stars in the galaxy likely formed in globular clusters, and very little to no “normal” low-density star formation occurred. This result implies that the most extreme conditions during early galaxy formation promoted star formation in massive and dense clumps, in contrast to the dispersed star formation observed in galaxies today.

Unified Astronomy Thesaurus concepts: [Low surface brightness galaxies \(940\)](#); [Globular star clusters \(656\)](#); [Galaxy formation \(595\)](#); [Star formation \(1569\)](#); [Hubble Space Telescope \(761\)](#); [HST photometry \(756\)](#); [Observational astronomy \(1145\)](#); [Dwarf galaxies \(416\)](#); [Star clusters \(1567\)](#)

1. Introduction

Star formation in the Milky Way typically proceeds in molecular clouds with sizes of 10–100 pc, leading to loose conglomerations of stars that slowly disperse within the Galaxy (Kennicutt & Evans 2012). Star formation can also produce compact, gravitationally bound systems (Krumholz et al. 2019), the most massive of which become long-lived globular clusters (Kruijssen 2014). This mode of star formation is rare because it requires extreme gas pressures, $P/k > 10^6 \text{ K cm}^{-3}$ (Elmegreen & Efremov 1997; Kruijssen 2015), causing globular clusters to contain less than 0.5% of the stars in most present-day galaxies (Forbes et al. 2018).

Nonetheless, the specific frequency (S_N), the total number of clusters per unit galaxy luminosity, can differ by a factor of ~ 40 – 50 between individual galaxies, with the largest specific frequencies observed at the very lowest or very highest luminosities (Miller & Lotz 2007; Harris et al. 2013).

Alongside their extended sizes and low surface brightnesses, some ultra-diffuse galaxies (UDGs; van Dokkum et al. 2015) stand out by their elevated globular cluster abundances and the high specific frequencies compared to other galaxies with the same luminosities (Peng & Lim 2016; van Dokkum et al. 2017; Lim et al. 2020 and references therein). One proposed explanation is that UDGs formed at earlier times than typical dwarf galaxies in higher surface density environments typical of these epochs, giving rise to a larger fraction of their stellar mass formed in gravitationally bound clusters (e.g., Carleton et al. 2021; Trujillo-Gomez et al. 2021).

In particular, one such extremely globular cluster-rich UDG is NGC 5846-UDG1. It was first cataloged in a photometric survey targeting the area surrounding the NGC 5846 group with the Canada–France–Hawaii Telescope (Mahdavi et al. 2005) and was recently reidentified in the VEGAS survey (Forbes et al. 2019), showing a collection of globular clusters at its center. Follow-up spectroscopic observations with the Very Large Telescope multi-unit spectroscopic explorer confirmed that at least 11 of the globular clusters are associated with NGC 5846-UDG1 based on their radial velocities (Müller et al. 2020). The ground-based images lack the resolution to resolve the compact sources and therefore reliably determine the actual size of NGC 5846-UDG1’s globular cluster population.

¹² NASA Hubble Fellow.

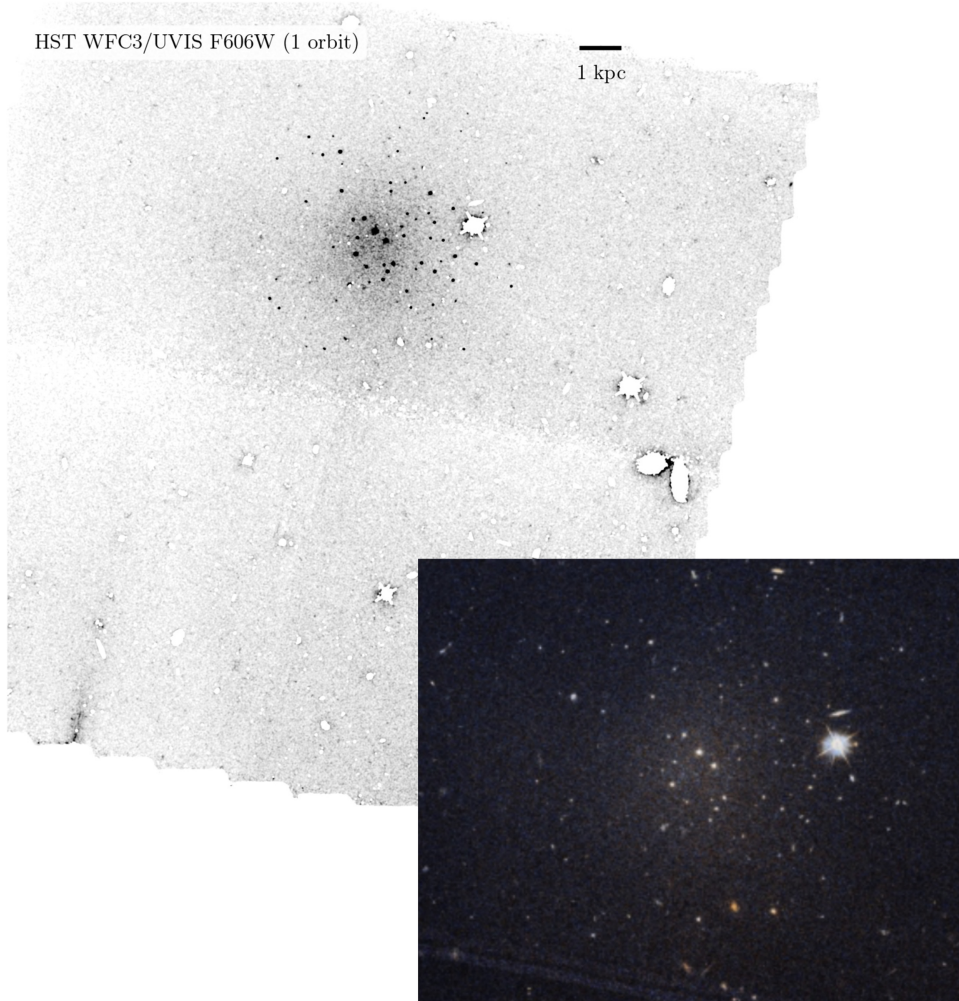


Figure 1. Upper image: V -band image taken with the WFC3 UVIS channel. All sources are masked except for the smooth diffuse light component of NGC 5846-UDG1 and its globular cluster candidates. About 13% of all stars reside in NGC 5846-UDG1’s globular clusters, and both components have similar spatial distributions. Lower right image: F606W–F475W combined color image. Globular clusters brighter than $M_{F606W} = -7.6$ mag have a median $g - V$ color of $F475W - F606W = 0.4$ mag and very little spread ($\sigma_{F475W - F606W} = 0.03$ mag), suggesting similar ages and chemical compositions.

Müller et al. (2021)¹³ used single-orbit Hubble Space Telescope Advanced Camera for Surveys (HST/ACS) observations and identified 26 ± 6 globular clusters associated with NGC 5846-UDG1.

In this Letter, we present an analysis of NGC 5846-UDG1 and its globular cluster system using new, deeper observations with HST Wide Field Camera 3 (WFC3). We find a larger number of globular clusters than previous studies and that cluster stars make up a remarkably high fraction of the total number of stars in the galaxy. We model NGC 5846-UDG1’s initial cluster mass function (ICMF) as a function of the birth galactic environment and discuss the implications of our results for different modes of star formation in the early universe.

2. Observations and Analysis

2.1. HST Imaging

NGC 5846-UDG1 was observed with WFC3/UVIS on 2020 December 27, in Cycle 28 (program GO-16284; PI: Danieli). The program focused on characterizing the

numerous compact sources in the vicinity of NGC 5846-UDG1 by obtaining deep images of the galaxy in two filters. Two orbits were obtained with total exposure times of 2349 and 2360 s in F475W and F606W, respectively. As the aim was to resolve individual globular clusters potentially associated with NGC 5846-UDG1, the WFC3 was selected to exploit its improved resolution ($0''.04 \text{ pixel}^{-1}$) over the ACS. The drizzled `drc` images produced by the STScI standard pipeline were used in the analysis. The HST images were primarily used for the identification and characterization of the globular clusters in NGC 5846-UDG1. The data were also used for isolating the low surface brightness component of the galaxy in the Dark Energy Camera Legacy Survey (DECaLS; Dey et al. 2019) for deriving NGC 5846-UDG1’s structural parameters (see below).

A color image generated from the HST F606W and F475W images is shown in the bottom panel of Figure 1. An abundant population of bright globular clusters is resolved with the HST/WFC3’s high resolution and can be seen clustered close to the center of the galaxy. A diffuse distribution of field stars is also detected. No other known galaxy has such a striking, dominant globular cluster population.

¹³ Müller et al. (2021) referred to NGC 5846-UDG1 as MATLAS-2019.

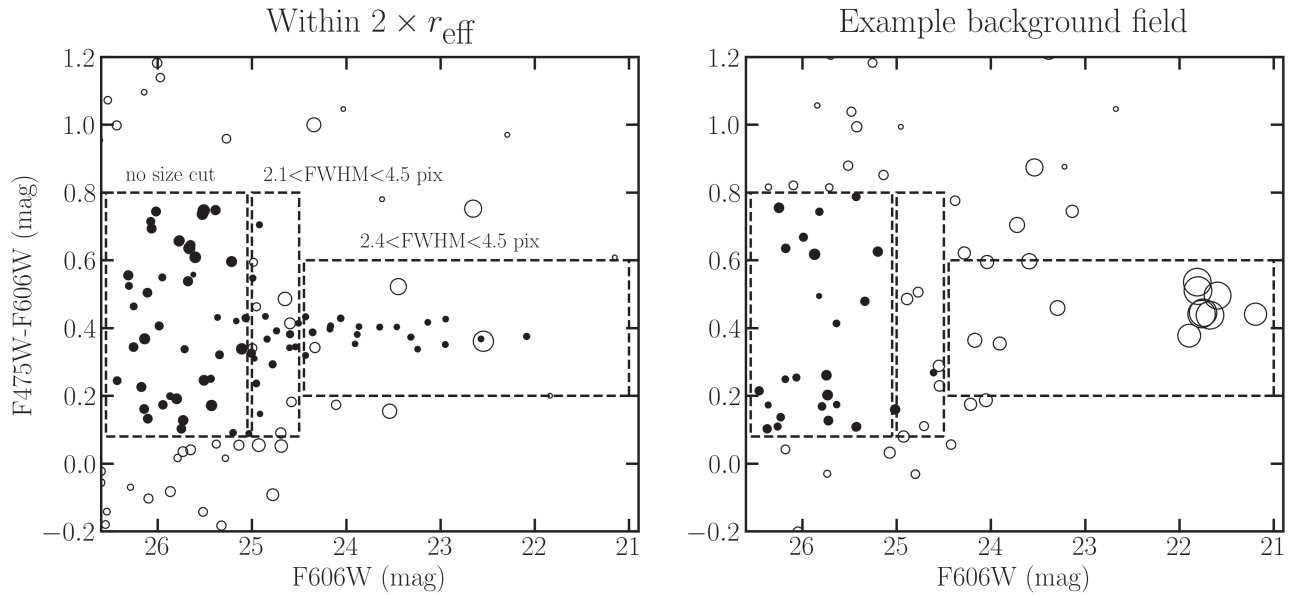


Figure 2. Photometric selection criteria for globular clusters in NGC 5846-UDG1. Left panel: all sources within $2 \times r_{\text{eff}}$ in the color–magnitude plane. All sources have sizes proportional to their FWHM sizes measured in pixels. Sources that met the selection criteria are shown by filled circles, and open circles are sources that were not selected. The three dashed boxes show the different color criteria as a function of the F606W magnitude. Right panel: same as the left panel for a background field with a similar area. There is only one contaminating source (filled circle) with $m_{\text{F606W}} < 25.0$ mag. For fainter sources ($m_{\text{F606W}} > 25.0$ mag), the number of contaminating objects increases, and these are accounted for in the calculation of the total globular cluster number.

2.2. Identification of Globular Clusters

Identification of the globular clusters in NGC 5846-UDG1 is based on their appearance in the two-orbit WFC3/UVIS images. We also utilize the information of the 11 spectroscopically confirmed globular clusters as detailed below.

First, SExtractor (Bertin & Arnouts 1996) is run on the F606W and F475W drizzled images in dual-image mode, where detection is done on the F606W images with a threshold of 6 connected pixels at a level of 2σ (DETECT_THRESH = 2σ and DETECT_MINAREA = 6 pixels). This results in a 5σ threshold for a group of 6 connected pixels to be detected as an object. While this choice of SExtractor parameters was made to also allow the detection of clusters fainter than the turnover magnitude, it is still very conservative compared to past studies that used similar detection techniques with detection thresholds in the 2σ – 3.5σ regime, compared to our 5σ threshold (e.g., Jordán et al. 2004; Beasley & Trujillo 2016).

The photometry is corrected for Galactic extinction (Schlafly & Finkbeiner 2011). Total magnitudes were determined using the “AUTO” fluxes from SExtractor corrected to an infinite aperture using the up-to-date UVIS2 encircled energy corrections.¹⁴ All magnitudes are given in the AB system. The F475W–F606W color correction is negligible, and therefore no correction was required for the wavelength dependence of the point-spread function (PSF).

Similar to past studies (van Dokkum et al. 2018; Shen et al. 2021), globular cluster selection is done from the HST photometry using a set of size and color criteria. The selection is informed by the color and size distributions of the 11 spectroscopically confirmed globular clusters with $(\mu, \sigma)_{\text{F475W-F606W}} = (0.39, 0.03)$ mag and $(\mu, \sigma)_{\text{FWHM}} = (2.9, 0.29)$ pixels. We apply varying color and size criteria for

different magnitude-selected sources to account for the variation in the photometric uncertainties with magnitude.

Similar to van Dokkum et al. (2018) and Shen et al. (2021), we create three size- and color-selected source catalogs as demonstrated in Figure 2. We measure the half-light radius of the galaxy (r_{eff} ; see Section 3) and use the same selection criteria when generating source catalogs for the galaxy (within $2 \times r_{\text{eff}}$) and a background field (outside $3 \times r_{\text{eff}}$). The background field is used for correcting for contaminating background and foreground sources. The first catalog includes sources brighter than $m_{\text{F606W}} = 24.5$ mag and within a narrow color and size range of $0.2 \text{ mag} < \text{F475W} - \text{F606W} < 0.6 \text{ mag}$ and $2.4 \text{ pixels} < \text{FWHM} < 4.5 \text{ pixels}$, respectively (rightmost dashed box). The same selection is made on sources that are outside $3 \times r_{\text{eff}}$ for background subtraction. Using these criteria, we find 20 sources within $2 \times r_{\text{eff}}$ and two sources outside $3 \times r_{\text{eff}}$. Accounting for the relative area differences ($A_{\text{bg}} = 6.7 \times A_{\text{gal}}$), this first catalog has a background contamination of 0.3 sources within $2 \times r_{\text{eff}}$. We repeat the same procedure for fainter sources using two more selection criteria. For sources with $24.5 \text{ mag} < m_{\text{F606W}} < 25.0 \text{ mag}$, we allow a wider color range criterion of $0.08 \text{ mag} < \text{F475W} - \text{F606W} < 0.8 \text{ mag}$ and $2.1 \text{ pixels} < \text{FWHM} < 4.5 \text{ pixels}$ (middle dashed box). We identify 13 sources within $2 \times r_{\text{eff}}$ and 0.7 background contaminants. Finally, for sources with $25.0 \text{ mag} < m_{\text{F606W}} < 26.5 \text{ mag}$, we apply the same color cut of $0.08 \text{ mag} < \text{F475W} - \text{F606W} < 0.8 \text{ mag}$ and no size cut (leftmost dashed box). The final selection adds a total of 43 sources inside $2 \times r_{\text{eff}}$ and 24.5 background contaminants. The left panel of Figure 2 shows all sources within $2 \times r_{\text{eff}}$ from the center of the galaxy, with circle sizes proportional to their FWHM sizes measured with SExtractor. Open circles represent sources that were not selected, and filled circles are sources that meet both the color and size criteria for their F606W magnitude. The right panel shows the same selection applied to an example background field. The contamination for the

¹⁴ <https://www.stsci.edu/hst/instrumentation/wfc3/data-analysis/photometric-calibration/uvis-encircled-energy>

bright source catalog is very low, with essentially no contaminating sources below $m_{F606W} < 24.5$ mag.

In total, we find a background-corrected number of 50.4 globular clusters within $2 \times r_{\text{eff}}$. Assuming a Sérsic distribution of the globular clusters with the same Sérsic index for the smooth light component ($n = 0.61$; see Section 3) and half-light radius, we estimate that three more globular clusters should reside outside $2 \times r_{\text{eff}}$. We also correct for sources fainter than 26.5 mag, assuming a Gaussian distribution and adopting the best-fit mean and scatter of $\mu = 24.7$ and $\sigma = 1.1$ mag (see Section 4). Together, we obtain 53.9 ± 8.9 globular clusters associated with NGC 5846-UDG1. The uncertainty in the total globular cluster count is dominated by the number of background sources at the faint end of the luminosity function and reflects Poisson errors in the observed counts (galaxy – background). Brighter than $m_V \sim 24.5$ mag, just fainter than the turnover magnitude, the background contamination is extremely small (as demonstrated in Figure 2), resulting in small error bars on the number counts of the clusters in these bins. Fainter than ~ 24.5 mag, the uncertainty increases due to the increasing background contamination levels. We note that objects identified using our selection (50.4) make up 93.5% of the estimated total globular cluster count in NGC 5846-UDG1. Thus, work such as Saifollahi et al. (2021), claiming that corrections may bias the estimated globular cluster numbers, is not applicable in the case of NGC 5846-UDG1, which resides at a much closer distance, where the correction is at the $\sim 5\%$ – 10% level.

A lower globular cluster count in NGC 5846-UDG1 was previously determined using ground-based data (~ 45 , no error bars provided; Forbes et al. 2021) and also using slightly shallower, single-orbit HST/ACS data (Müller et al. 2021). Müller et al. (2021) reported 26 ± 6 globular clusters, compared to 54 ± 9 found here. We suspect that the difference in depth (two versus one orbit) and sampling ($0''.04 \text{ pixel}^{-1}$ with WFC3 compared to $0''.05 \text{ pixel}^{-1}$ with ACS) between the data sets may be indirectly responsible for the difference. With the information provided in Müller et al. (2021), we were not able to perform a direct comparison with our analysis. The SExtractor parameter choices in Müller et al. (2021; DETECT_THRESH = 2σ and DETECT_MINAREA = 6 pixels) result in a 6.7σ detection threshold criterion. We repeat our analysis with these SExtractor parameters and find that it results in a decrease of 10 sources (from 50.3 to 40.1 clusters within $2R_{\text{eff},*}$, corrected for interlopers); all are fainter than 25 mag, below the turnover magnitude. This quite restrictive criterion (6.7σ) used in Müller et al. (2021) likely excludes the smallest and faintest sources from their analysis. As shown below, this decrease in the background-corrected number of faint objects has no effect on our conclusions.

3. Structural and Physical Parameters

NGC 5846-UDG1 is located in the NGC 5846 galaxy group at a projected distance of $21'$ from NGC 5846 itself. It has a radial velocity of $2167 \pm 2 \text{ km s}^{-1}$ (Forbes et al. 2021), consistent with it being a member of the group, which has a mean velocity of 1828 km s^{-1} and a velocity dispersion of $\sim 295 \text{ km s}^{-1}$ (Müller et al. 2020). We use the i -band image from the Hyper Suprime-Cam Subaru Strategic Program PDR2 (Aihara et al. 2019) to measure the surface brightness fluctuation (SBF) distance to NGC 5846-UDG1. The SBF signal is measured using techniques developed for dwarf

galaxies, with a calibration of $\bar{M}_i = -1.29 \pm 0.22$ mag based on the color of NGC 5846-UDG1, as described in Carlsten et al. (2019) and Greco et al. (2021). We measure an SBF magnitude of $\bar{M}_i^{\text{UDG1}} = 30.3 \pm 0.5$ mag, which places NGC 5846-UDG1 at $D \sim 21 \pm 5$ Mpc. This is consistent with the distance to the NGC 5846 group of 26.5 ± 0.8 Mpc reported in Kourkchi & Tully (2017) based on the weighted average distance of any members available in the Cosmicflows-3 distance catalog (Tully et al. 2016). We adopt $D = 26.5$ Mpc as the distance to NGC 5846-UDG1 due to the low signal-to-noise ratio (S/N) achieved using the SBF technique, which places it at a projected distance of 162 kpc from NGC 5846. We note that the main result of the paper, namely, the globular cluster-to-field stars fraction, as shown below, is very insensitive to the exact distance to NGC 5846-UDG1.

Using HST and DECaLS data in tandem, we characterize the galaxy’s physical and structural properties. The size, luminosity, surface brightness, and stellar mass of NGC 5846-UDG1 were derived using the DECaLS images. Attempts were made to use the HST images for this purpose, but the galaxy’s surface brightness is too low for reliably fitting it with a model image. Instead, we utilized the HST images in a different way. We used the multi-resolution filtering (MRF) software (van Dokkum et al. 2020) to remove all compact sources from the DECaLS images and isolate the diffuse component of NGC 5846-UDG1. Briefly, SExtractor was run on the high-resolution HST images, and the resulting segmentation map was converted to a mask and multiplied by the image to create a flux model of all detected sources. Low surface brightness objects and saturated stars were removed from this model. The model was then convolved with a kernel to match the DECaLS PSF and subtracted. The original r -band DECaLS and final residual image binned 2×2 , conserving only the low surface brightness component, are shown in the left two panels of Figure 3.

Next, we parameterized the galaxy’s structure by fitting a two-dimensional Sérsic model to the smooth light component in the DECaLS g - and r -band images. We used the `pymfit`¹⁵ code, a python wrapper of `imfit` (Erwin 2015), on the MRFed; masked; and binned (2×2) DECaLS images. First, `imfit` was run on the r -band MRFed image to determine the structural parameters of the galaxy and its brightness. Then, the g -band MRFed image was fitted while allowing only the amplitude to change. To estimate the galaxy fit uncertainties, we injected the best-fit `imfit` model into different areas in the MRFed and binned g and r images, and then we fitted the injected models in the same way we fitted the galaxy. We adopt the rms variation in the fitted parameters as the uncertainty for each parameter. The final model and residual r -band image are shown in the right two panels of Figure 3.

The best-fit model has a Sérsic index of $n = 0.6$, axis ratio $b/a = 1.0$, and a central surface brightness of $\mu_{g,0} = 25.4 \text{ mag arcsec}^{-2}$. It has a half-light radius of $r_{\text{eff}} = 15''.6$, corresponding to $r_{\text{eff}} = 1.9 \text{ kpc}$ at 26.5 Mpc. We transform the g - and r -band measured quantities into V -band magnitude and luminosity.¹⁶ Its total V -band absolute magnitude is $M_V = -14.6$ mag, and its luminosity is $L_V = 5.9 \times 10^7 L_{\odot}$. With a mass-to-light ratio $M/L_V = 2.0$,

¹⁵ <https://github.com/johnnygreco/pymfit>

¹⁶ <http://www.sdss3.org/dr8/algorithms/sdssUBVRITransform.php#Lupton2005>

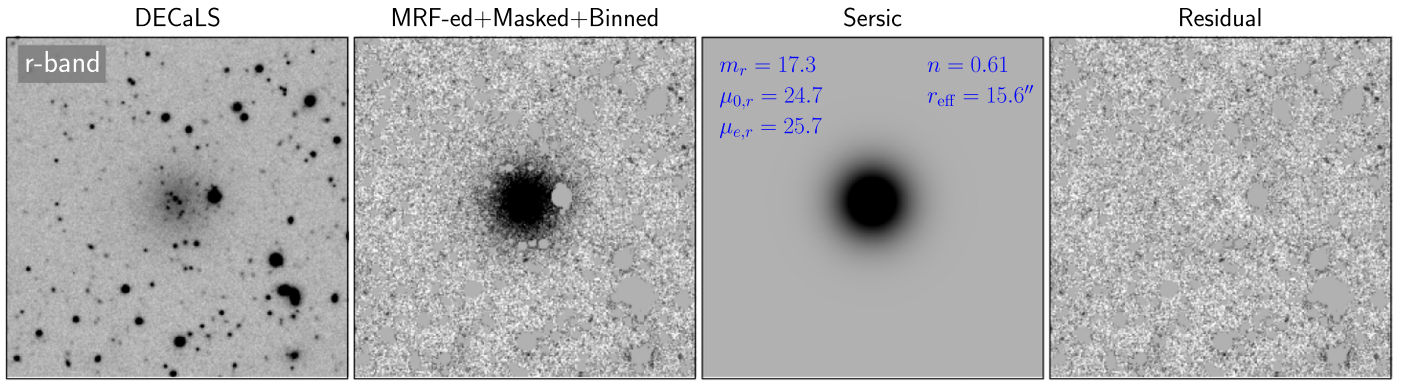


Figure 3. First panel (from left to right): $47'' \times 47''$ DECaLS r -band cutout centered on NGC 5846-UDG1. Second panel: same cutout after MRF. High surface brightness and compact sources were subtracted and masked. Third panel: two-dimensional Sérsic best-fit model obtained using the `pymfit` code. The best-fit model parameters are shown in the blue text. Fourth panel: residual image after subtracting the galaxy model.

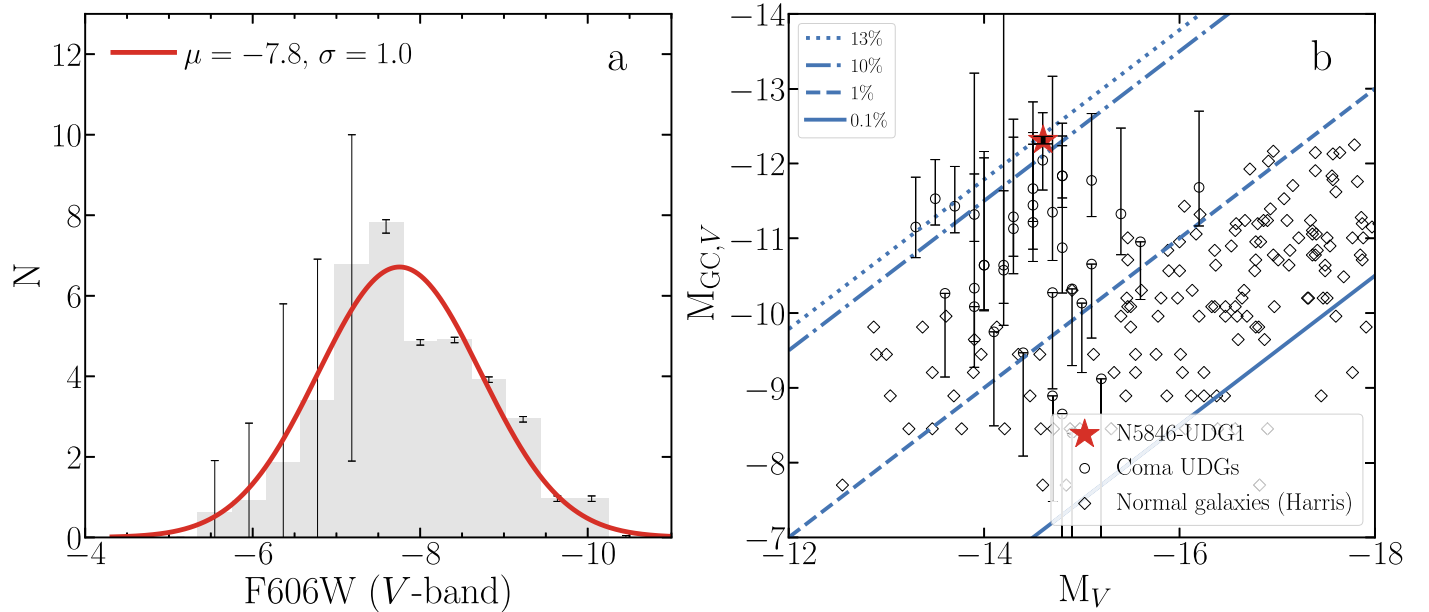


Figure 4. Left panel: background-subtracted globular cluster luminosity function of NGC 5846-UDG1 in absolute magnitude (gray histogram) and its best-fit Gaussian luminosity function (red curve). Right panel: absolute magnitude in globular clusters vs. total magnitude of the host galaxy. Diagonal lines show constant globular cluster-to-field star light fractions ranging from 0.1% to 13%. Shown by a red star, NGC 5846-UDG1 has the highest fraction of stars in globular clusters known to date ($12.9\% \pm 0.6\%$). This is measured with high certainty, demonstrated with the small error bar (0.05 mag) on top of the star. Some Coma UDGs (open circles) are excellent candidates for sharing a similar high fraction of stars in globular clusters, but these are four times farther away and thus 16 times fainter and have commensurately larger error bars.

based on $[\text{Fe}/\text{H}] = -1.33$ and age = 11.2 Gyr from Müller et al. (2020), we obtain a stellar mass of $M_* \approx 1.2 \times 10^8 M_\odot$.

4. Fraction of Stars in Globular Clusters

In the left panel of Figure 4, we show the globular cluster luminosity function and a best-fit Gaussian function. Assuming a distance of 26.5 Mpc, it peaks at $M_V = -7.5$ mag with a width of $\sigma = 1.1$ mag, consistent with canonical values for globular cluster systems in most other galaxies (Rejkuba 2012).

We calculate the fraction of light in globular clusters relative to the total light of the galaxy. The total flux in globular clusters was obtained by integrating the F606W and F475W histograms (scaled to account for the background subtraction). We calculate the 1σ and 3σ uncertainties of the integrated globular cluster magnitude by generating 100,000 realizations of the histograms and calculating the 1σ (16%, 84%) and 3σ (0.15%, 99.8%) intervals of the total magnitude distribution. Each

histogram is created by perturbing the measured histogram values according to the error bars in each bin for magnitude bins fainter than $M = -7.5$ mag. The total light in the identified globular clusters is dominated by the most massive clusters and is therefore insensitive to the completeness limits.

We find that the fraction of light in globular clusters is unusually high given the galaxy total absolute magnitude, with $M_{V,\text{GCs}} = -12.5 \pm 0.05$ mag. This implies that $12.9\% \pm 0.6\%$ of the stars (measured in the V band) currently reside in the globular clusters, a fraction that is about $100\times$ greater than that for the Milky Way (Harris et al. 2013). We note that the M_V/L_V measured by Müller et al. (2020) for the field stars ($2.0^{+0.3}_{-0.1} M_\odot/L_\odot$) and globular clusters ($1.6^{+0.3}_{-0.1} M_\odot/L_\odot$) thusing their stacked spectra are consistent within the errors. This is also true for the M_V/L_V measured for individual clusters (though with a significantly lower S/N). If we adopt $2.0^{+0.3}_{-0.1} M_\odot/L_\odot$ for the field stars and $1.6^{+0.3}_{-0.1} M_\odot/L_\odot$ for the globular clusters, we get that 10.3% of the stars are in globular

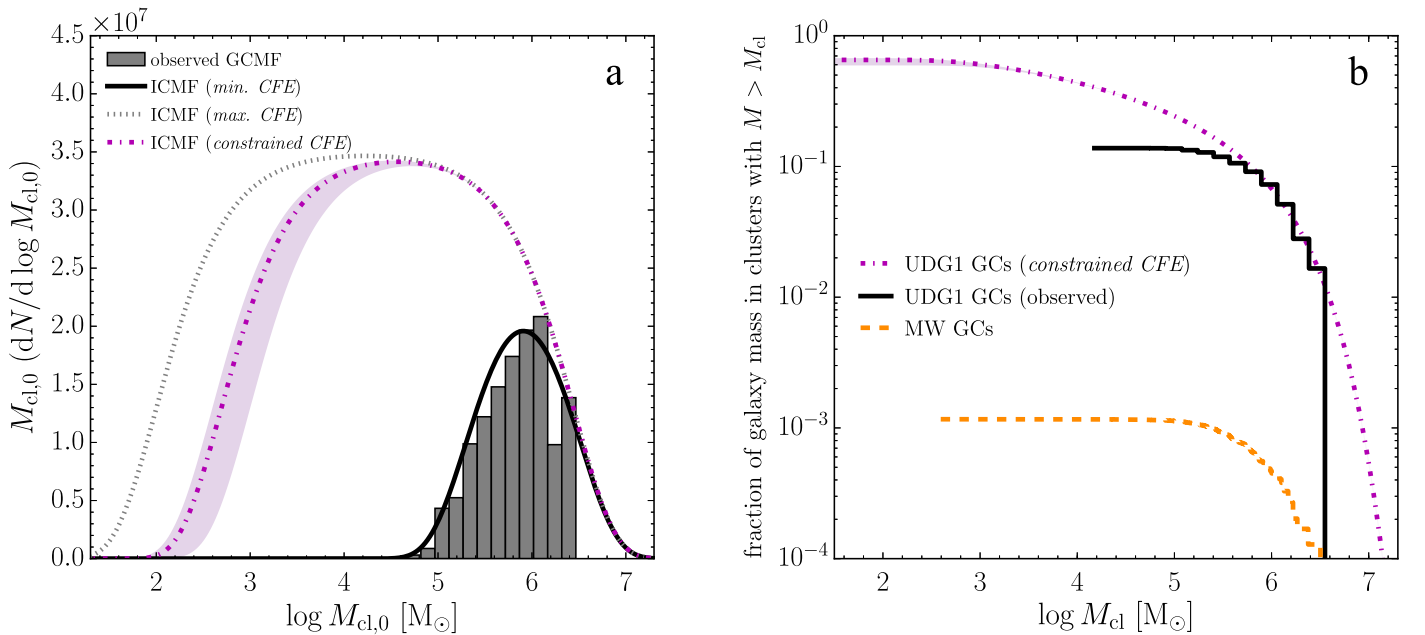


Figure 5. The ICMF models constrain the origin of NGC 5846-UDG1’s globular cluster system. Left panel: constraints on the ICMF of NGC 5846-UDG1, based on its present-day observed globular clusters and total stellar mass. The observed GCMF, corrected for mass loss due to stellar evolution, is shown by the black histogram. The fiducial model, constrained by the environmental dependence of the fraction of star formation in bound clusters (i.e., the CFE; Kruijssen 2012), is shown as the shaded purple band for a range of Toomre Q disk stability parameters ($0.5 \leq Q \leq 3.0$), where the purple dotted–dashed curve corresponds to $Q = 0.5$. For reference, the black solid and dashed gray curves show the minimum and maximum CFE models. The minimum CFE model assumes that the present-day globular clusters were the only clusters that formed, whereas the maximum CFE model assumes that all stars in the galaxy came from disrupted low-mass clusters. The mass functions are weighted by mass, so that the area under each curve is directly proportional to the mass in clusters. Right panel: cumulative fraction of galaxy mass in clusters at the time of formation for NGC 5846-UDG1 in comparison to the Milky Way. For NGC 5846-UDG1, the purple dotted–dashed curve shows the fiducial model (constrained by the CFE), and the black solid curve shows the present-day observed fraction. The orange dashed curve assumes no mass loss or cluster disruption for the Milky Way globular clusters, correcting only for mass loss due to stellar evolution. The fraction of galaxy mass in clusters in NGC 5846-UDG1 is 2–3 orders of magnitude higher than in the Milky Way, irrespective of the adopted CFE model.

clusters. Lastly, adopting the Müller et al. (2021) 6.7σ SExtractor object detection threshold (instead of our 5σ threshold; see Section 2.2), the globular cluster-to-field star ratio changes from 12.9% to 12.1%, which has no effect on our conclusions, as discussed below.

5. Discussion

5.1. Modeling of the Cluster-to-Field Star Mass Ratio

NGC 5846-UDG1 is the first known galaxy with a present-day globular cluster-to-field star mass ratio that is $\geq 10\%$ with $>90\%$ confidence. Fractions that are this high have important implications for formation models of the galaxy while providing new constraints on globular cluster mass loss. On long-enough timescales, clusters across all masses evolve dynamically, including the complete dissolution of low-mass clusters. These processes include tidal shocks through interactions with the substructure of the dense interstellar medium and evaporation as a result of two-body relaxation (Krause et al. 2020). Taking into account the complete destruction of low-mass coeval proto-globular clusters, as well as mass loss from the surviving clusters, it is thought that the cluster population initially contained up to a factor of a few more stars than are observed after ~ 10 Gyr. That is, globular cluster systems could lose up to $\sim 80\%$ – 90% of their stars over their lifetime (Larsen et al. 2012; Kruijssen 2015; Reina-Campos et al. 2018). With a measured fraction of $12.9\% \pm 0.6\%$, NGC 5846-UDG1 could have started with a globular cluster-to-field star mass fraction approaching 100%. Below, we quantify this result using the specific properties of NGC 5846-UDG1.

We apply an analytical physical model to the present-day globular cluster mass function (GCMF). The model, described in Trujillo-Gomez et al. (2019), infers the environmental conditions within the progenitor galaxy and the cluster formation efficiency (CFE, the fraction of star formation occurring in gravitationally bound clusters; Kruijssen 2012) at the time of formation. In particular, the model relates the properties of the host galaxy disk at the time of formation (its gas surface density, rotational angular velocity, and Toomre Q stability parameter) to the minimum and maximum cluster masses (Reina-Campos & Kruijssen 2017; Trujillo-Gomez et al. 2019) of the ICMF, as well as the CFE. Together with the assumption of a power-law slope of -2 between the minimum and maximum exponential truncation masses, these quantities completely determine the double-Schechter ICMF (Trujillo-Gomez et al. 2019; Adamo et al. 2020). We assume $M/L_V \approx 2.0$ and correct for the fractional mass loss due to stellar evolution of $f = 0.35$ for the field stars and $f = 0.40$ for the globular clusters to also account for mass segregation (Lamers et al. 2010). This model accurately reproduces the demographics of young and old cluster populations in the local universe (Pfeffer et al. 2019; Trujillo-Gomez et al. 2019).

The left panel of Figure 5 shows the ICMF for the two end-cases for the inferred fraction of the total stars formed in bound clusters. The black solid curve shows the minimum CFE case, where only the stars currently observed in clusters were born in gravitationally bound clusters, and the ICMF is simply the present-day GCMF corrected for mass loss due to stellar evolution (i.e., with no dynamical mass loss). The gray dashed curve shows the maximum CFE case, where all of the stars in

the galaxy were born in bound clusters and assuming that the integrated ICMF mass cannot exceed the total stellar mass of the galaxy. These two cases bracket the range of possibilities.

To obtain a self-consistent solution for the ICMF and star-forming environment of the galaxy, we then apply the ICMF and the CFE models (Trujillo-Gomez et al. 2019 and Kruijssen 2012, respectively) to the GCMF of NGC 5846-UDG1. The modeling procedure is thoroughly described in Trujillo-Gomez et al. (2019); here we summarize it briefly.

1. The present-day GCMF is fitted with a power law with a double exponential truncation at the minimum and maximum cluster masses, determining M_{\max} and the largest possible value of M_{\min} .
2. The total mass formed in clusters can be calculated in two ways.
 - (a) Using the product of the CFE and the galaxy stellar mass. This value depends on gas surface density, angular speed, and Q .
 - (b) Integrating the total mass under the ICMF. This value depends on the same variables as the CFE.

Assuming that we know M_{\max} (from step 1), we search the parameter space of Σ_{ISM} , Ω , and M_{\min} for solutions to the following equation (from Trujillo-Gomez et al. 2019), which relate (a) and (b):

$$\Gamma^{\text{K12}}(\Sigma_{\text{ISM}}, \Omega, Q) = \frac{\int_0^\infty \text{ICMF}(M_{\min}, M_{\max}, M) M dM}{M_{\star, \text{UDG1}}}. \quad (1)$$

This determines M_{\min} and the interstellar medium (ISM) conditions that produced the globular clusters.

The purple band shows the self-consistent fiducial ‘‘constrained CFE’’ model, which uses this additional requirement that the predicted set of environmental properties simultaneously reproduces the observed minimum and maximum masses, and the predicted fraction of star formation in bound clusters. The fiducial model is shown for a disk stability range of $0.5 \leq Q \leq 3.0$, where the purple dotted–dashed curve corresponds to $Q = 0.5$. We note that the fiducial constrained CFE model is the only physical solution for the ISM conditions and the CFE. We refer the reader to Trujillo-Gomez et al. (2019) for a detailed description of the model.

Adopting a Toomre Q disk stability value of $Q = 0.5$, which reflects the typical values observed in high-redshift galaxies (Genzel et al. 2014), the physical solution, namely, the constrained CFE model, yields a minimum cluster mass of $M_{\min} = 4.9 \times 10^2 M_\odot$ and a bound fraction of $65\% \pm 2\%$. This implies that to satisfy the ISM conditions required to produce the observed GCMF (gas surface density $\Sigma_{\text{ISM}} = 4.2 \pm 0.6 \times 10^2 M_\odot \text{pc}^{-2}$ and shear $\Omega = 0.24^{+0.18}_{-0.10} \text{Myr}^{-1}$), a very large fraction of the total mass of NGC 5846-UDG1 had to form in bound clusters. We therefore infer that it is likely that most of the star formation in NGC 5846-UDG1 happened in extremely dense cluster-forming gas clumps (in order to produce clusters that remain bound after losing their gas), with unusually little low-density (i.e., unbound) star formation occurring.¹⁷

The right panel of Figure 5 shows the cumulative fraction of galaxy mass in clusters at formation for NGC 5846-UDG1 in comparison to the Milky Way (orange dashed curve), assuming no cluster mass loss or disruption for the Milky Way (i.e., the

minimum CFE case); $M/L_V = 2.0$ is assumed for the Milky Way globular clusters (Harris 1996) and a stellar mass of $M_\star^{\text{MW}} = 5 \times 10^{10} M_\odot$ (Bland-Hawthorn & Gerhard 2016). The black solid curve is the minimum CFE case for NGC 5846-UDG1, while the purple dotted–dashed curve shows the fiducial model. There is a 2–3 orders of magnitude difference between NGC 5846-UDG1 and the Milky Way, further demonstrating the extraordinary conditions that led to the formation of NGC 5846-UDG1. While formation in massive, gravitationally bound clusters made only minor contributions to the total Milky Way mass, star formation in dense clumps is the dominant formation channel in NGC 5846-UDG1.

5.2. Tests of the Model

How can this scenario be further tested observationally? If indeed a large fraction of the field stars came from dissolved clusters, then the expectation is that both the stellar populations (particularly the ages) and the spatial distribution of the field stars and globular clusters are similar. In other galaxies, this is typically not the case, with globular clusters, on average, being more metal-poor and older than field stars, and their spatial distribution is more extended, with $R_{\text{eff,GC}} \approx 1.5\text{--}2R_{\text{eff},\star}$ (Kantha et al. 2014; van Dokkum et al. 2017; Lim et al. 2018). Recent spectroscopic data have shown that the globular clusters and field stars of NGC 5846-UDG1 have consistent ages (with age = $11.2^{+1.8}_{-0.8}$ Gyr for the field stars and age = $9.1^{+3.0}_{-0.8}$ Gyr for the globular clusters) and metallicities ($[\text{Fe}/\text{H}] = -1.33^{+0.19}_{-0.01}$ for the field stars and $[\text{Fe}/\text{H}] = -1.44^{+0.10}_{-0.07}$ for the globular clusters; Müller et al. 2020). We measure the half-number radius of the globular clusters by selecting all sources from the entire HST image that have V-band magnitudes brighter than 25 mag (fainter than the expected canonical peak at 24.6 mag), are relatively compact ($2.2 \text{ pixels} < \text{FWHM} < 5.0 \text{ pixels}$), and have $g - V$ colors between 0.2 and 0.6 mag. We identify 34 globular clusters in the sample, of which 31 are located very close to the galaxy. With this low-contamination sample ($N_{\text{contamination}} = 0.15$ clusters), we find $R_{\text{eff,GC}} = 12''.6 \pm 1''.8$, consistent with the field star half-light radius of $R_{\text{eff}} = 15''.6 \pm 0''.8$. The similar (and possibly more concentrated) distribution of globular clusters compared to the smooth stellar distribution, as well as the similar ages and chemical compositions, supports a common origin of the stars in globular clusters and field stars. Future studies may be able to refine the age estimates of the clusters and the diffuse light.

5.3. NGC 5846-UDG1 in Context

It is likely that NGC 5846-UDG1 is not alone. Globular cluster–rich UDGs have been identified and studied in various cosmic environments (Beasley & Trujillo 2016; van Dokkum et al. 2017; Forbes et al. 2020; Somalwar et al. 2020). In fact, the large population of globular clusters in such low-luminosity and diffuse systems has been one of the properties that make the formation of UDGs stand out as perplexing in the context of modern physical models of galaxy formation. We put NGC 5846-UDG1 in context with other globular cluster–rich galaxies with absolute magnitudes ranging between $M_V = -12$ and -18 mag. In the right panel of Figure 4, we show the total V-band absolute magnitude of galaxies as a function of the total absolute magnitude of globular clusters in these galaxies. NGC 5846-UDG1 has a larger confirmed fraction of luminosity in its globular cluster system than any of the other galaxies. Interestingly, some UDGs in the Coma cluster might possess

¹⁷ The model assumes that the majority of field stars and clusters formed during the same star formation episode.

similar extreme fractions of stars in their present-day globular cluster systems. However, the Coma cluster is located \sim four times farther than NGC 5846-UDG1; correspondingly, the uncertainties on the estimates of potentially associated globular clusters are much larger. These uncertainties are dominated by the high contamination from background and foreground objects at fainter magnitudes and the fact that their globular clusters are unresolved with HST at 100 Mpc. Nevertheless, these Coma galaxies suggest that clump-only star formation in galaxies may be quite common.

What conditions and processes might have promoted star formation predominantly in dense gas clumps, leading to the formation of a galaxy such as NGC 5846-UDG1? The ICMF model applied to NGC 5846-UDG1 predicts high gas surface densities ($\Sigma_{\text{ISM}} = 4.2 \pm 0.6 \times 10^2 M_{\odot} \text{pc}^{-2}$) at the time of formation. A recent model that connects the evolution of galaxies with their dark matter halos and globular cluster populations predicts that high globular cluster mass fractions arise naturally in early-collapsing dark matter halos due to their elevated gas surface densities at high redshift (Trujillo-Gomez et al. 2021). Such conditions give rise to massive cluster formation with a high CFE, resulting in an elevated number of globular clusters relative to the galaxy stellar mass. The model then predicts that the high clustering of the supernova feedback sources within the clusters could significantly increase the mass loading of gas outflows, which would lead to significant expansion of the stars and dark matter compared to galaxies with typical halo collapse times and globular cluster populations. For NGC 5846-UDG1, such a short-lived and efficient burst of star formation at high redshift may have also expelled the remaining gas, limiting star formation to this single event. The early-collapse UDG formation model predicts a correlation between the offset from the mean stellar mass–halo mass relation and the number of formed GCs. Precise constraints on the dark matter halo mass of NGC 5846-UDG1 could therefore be used to test this scenario. NGC 5846-UDG1 may be a case where star formation began like in many other galaxies but then failed to form stars in a low-density mode at later epochs.

We thank Jorge Moreno for providing helpful comments on the manuscript. Support from STScI grant HST-GO-16284 is gratefully acknowledged. S.D. is supported by NASA through Hubble Fellowship grant HST-HF2-51454.001-A awarded by the Space Telescope Science Institute, which is operated by the Association of Universities for Research in Astronomy, Inc., under NASA contract NAS5-26555. S.T.G. and J.M.D.K. gratefully acknowledge funding from the European Research Council (ERC) under the European Union’s Horizon 2020 research and innovation program via the ERC starting grant MUSTANG (grant agreement No. 714907). J.M.D.K. gratefully acknowledges funding from the Deutsche Forschungsgemeinschaft (DFG) in the form of an Emmy Noether Research Group (grant No. KR4801/1-1). S.T.G. gratefully acknowledges funding from the European Research Council (ERC) under the European Union’s Horizon 2020 research and innovation program via the ERC starting grant MUSTANG (grant agreement No. 714907). A.J.R. was supported by National Science Foundation grant AST-1616710 and as a Research Corporation for Science Advancement Cottrell Scholar.

ORCID iDs

Shany Danieli  <https://orcid.org/0000-0002-1841-2252>
 Pieter van Dokkum  <https://orcid.org/0000-0002-8282-9888>
 Sebastian Trujillo-Gomez  <https://orcid.org/0000-0003-2482-0049>
 J. M. Diederik Kruijssen  <https://orcid.org/0000-0002-8804-0212>
 Aaron J. Romanowsky  <https://orcid.org/0000-0003-2473-0369>
 Scott Carlsten  <https://orcid.org/0000-0002-5382-2898>
 Zili Shen  <https://orcid.org/0000-0002-5120-1684>
 Jiaxuan Li  <https://orcid.org/0000-0001-9592-4190>
 Roberto Abraham  <https://orcid.org/0000-0002-4542-921X>
 Jean Brodie  <https://orcid.org/0000-0002-9658-8763>
 Charlie Conroy  <https://orcid.org/0000-0002-1590-8551>
 Jonah S. Gannon  <https://orcid.org/0000-0002-2936-7805>
 Johnny Greco  <https://orcid.org/0000-0003-4970-2874>

References

- Adamo, A., Hollyhead, K., Messa, M., et al. 2020, *MNRAS*, 499, 3267
 Aihara, H., AlSayyad, Y., Ando, M., et al. 2019, *PASJ*, 71, 114
 Beasley, M. A., & Trujillo, I. 2016, *ApJ*, 830, 23
 Bertin, E., & Arnouts, S. 1996, *A&AS*, 117, 393
 Bland-Hawthorn, J., & Gerhard, O. 2016, *ARA&A*, 54, 529
 Carleton, T., Guo, Y., Munshi, F., Tremmel, M., & Wright, A. 2021, *MNRAS*, 502, 398
 Carlsten, S. G., Beaton, R. L., Greco, J. P., & Greene, J. E. 2019, *ApJ*, 879, 13
 Dey, A., Schlegel, D. J., Lang, D., et al. 2019, *AJ*, 157, 168
 Elmegreen, B. G., & Efremov, Y. N. 1997, *ApJ*, 480, 235
 Erwin, P. 2015, *ApJ*, 799, 226
 Forbes, D. A., Alabi, A., Romanowsky, A. J., Brodie, J. P., & Arimoto, N. 2020, *MNRAS*, 492, 4874
 Forbes, D. A., Bastian, N., Gieles, M., et al. 2018, *RSPSA*, 474, 20170616
 Forbes, D. A., Gannon, J., Couch, W. J., et al. 2019, *A&A*, 626, A66
 Forbes, D. A., Gannon, J. S., Romanowsky, A. J., et al. 2021, *MNRAS*, 500, 1279
 Genzel, R., Förster Schreiber, N. M., Rosario, D., et al. 2014, *ApJ*, 796, 7
 Greco, J. P., van Dokkum, P., Danieli, S., Carlsten, S. G., & Conroy, C. 2021, *ApJ*, 908, 24
 Harris, W. E. 1996, *AJ*, 112, 1487
 Harris, W. E., Harris, G. L. H., & Alessi, M. 2013, *ApJ*, 772, 82
 Jordán, A., Côté, P., Ferrarese, L., et al. 2004, *ApJ*, 613, 279
 Kartha, S. S., Forbes, D. A., Spitler, L. R., et al. 2014, *MNRAS*, 437, 273
 Kennicutt, R. C., & Evans, N. J. 2012, *ARA&A*, 50, 531
 Kourkchi, E., & Tully, R. B. 2017, *ApJ*, 843, 16
 Krause, M. G. H., Offner, S. S. R., Charbonnel, C., et al. 2020, *SSRv*, 216, 64
 Kruijssen, J. M. D. 2012, *MNRAS*, 426, 3008
 Kruijssen, J. M. D. 2014, *CQGra*, 31, 244006
 Kruijssen, J. M. D. 2015, *MNRAS*, 454, 1658
 Krumholz, M. R., McKee, C. F., & Bland-Hawthorn, J. 2019, *ARA&A*, 57, 227
 Lamers, H. J. G. L. M., Baumgardt, H., & Gieles, M. 2010, *MNRAS*, 409, 305
 Larsen, S. S., Strader, J., & Brodie, J. P. 2012, *A&A*, 544, L14
 Lim, S., Côté, P., Peng, E. W., et al. 2020, *ApJ*, 899, 69
 Lim, S., Peng, E. W., Côté, P., et al. 2018, *ApJ*, 862, 82
 Mahdavi, A., Trentham, N., & Tully, R. B. 2005, *AJ*, 130, 1502
 Miller, B. W., & Lotz, J. M. 2007, *ApJ*, 670, 1074
 Müller, O., Durrell, P. R., Marleau, F. R., et al. 2021, *ApJ*, 923, 9
 Müller, O., Marleau, F. R., Duc, P.-A., et al. 2020, *A&A*, 640, A106
 Peng, E. W., & Lim, S. 2016, *ApJL*, 822, L31
 Pfeffer, J., Bastian, N., Kruijssen, J. M. D., et al. 2019, *MNRAS*, 490, 1714
 Reina-Campos, M., & Kruijssen, J. M. D. 2017, *MNRAS*, 469, 1282
 Reina-Campos, M., Kruijssen, J. M. D., Pfeffer, J., Bastian, N., & Crain, R. A. 2018, *MNRAS*, 481, 2851
 Rejkuba, M. 2012, *Ap&SS*, 341, 195
 Saifollahi, T., Trujillo, I., Beasley, M. A., Peletier, R. F., & Knapen, J. H. 2021, *MNRAS*, 502, 5921
 Schlafly, E. F., & Finkbeiner, D. P. 2011, *ApJ*, 737, 103
 Shen, Z., van Dokkum, P., & Danieli, S. 2021, *ApJ*, 909, 179
 Somalwar, J. J., Greene, J. E., Greco, J. P., et al. 2020, *ApJ*, 902, 45

Trujillo-Gomez, S., Kruijssen, J. M. D., Keller, B. W., & Reina-Campos, M. 2021, [MNRAS](#), **506**, 4841
Trujillo-Gomez, S., Reina-Campos, M., & Kruijssen, J. M. D. 2019, [MNRAS](#), **488**, 3972
Tully, R. B., Courtois, H. M., & Sorce, J. G. 2016, [AJ](#), **152**, 50

van Dokkum, P., Abraham, R., Romanowsky, A. J., et al. 2017, [ApJL](#), **844**, L11
van Dokkum, P., Cohen, Y., Danieli, S., et al. 2018, [ApJL](#), **856**, L30
van Dokkum, P., Lokhorst, D., Danieli, S., et al. 2020, [PASP](#), **132**, 074503
van Dokkum, P. G., Abraham, R., Merritt, A., et al. 2015, [ApJL](#), **798**, L45